SELF-HEALING BEHAVIOR IN LOW-CARBON FIBER-REINFORCED CEMENTITIOUS COMPOSITES INCORPORATING CALCITE-COATED CELLULOSE

カルサイト被覆セルロースを用いた低炭素型繊維補強セメント系複合材料の自己修復特性

Efren John BUNO
エフレン ジョン ブーノ

A sustainable self-healing fiber-reinforced cementitious composite (FRCC) was developed by replacing 95% of cement with industrial by-products. This low-carbon FRCC (LCFRCC) achieved a 71% reduction in embodied carbon without compromising compressive strength. Self-healing was evaluated via watertightness recovery, specifically sorptivity and volume of permeable voids. Beyond cracking, LCFRCCs showed susceptibility to leaching during water immersion, which impairs watertightness. However, incorporating cellulose fibers coated with nanocalcite particles improved recovery in fly ash-rich systems. The efficacy of calcite-coated cellulose as a healing agent was demonstrated by a higher healing rate relative to the rate of natural matrix densification.

Keywords: *low carbon FRCC, autogenous self-healing, densification, cellulose fibers, nanocalcite*
低炭素 FRCC，自然自己修復，緻密化，セルロース繊維，ナノ炭酸カルシウム

1. Introduction

Concrete is the most widely used construction material due to its durability and cost-effectiveness. However, its inherently low tensile strength leads to inevitable cracking. In reinforced systems, these cracks facilitate the ingress of aggressive agents such as CO_2, Cl^-, and water, ultimately compromising structural integrity through steel corrosion. Notably, cracks narrower than 150 μm can naturally heal through the formation of calcite, a stable polymorph of calcium carbonate ($CaCO_3$)[1]. This process, known as autogenous self-healing, is important area of research in concrete technology for extending structural lifespans and reducing maintenance costs, particularly as sustainable and resilient infrastructure becomes central to modern disaster risk reduction strategies.

Fiber-reinforced cementitious composites (FRCC) effectively control crack widths and can enhance calcite growth up to 300 μm[2]. However, they typically require high volumes of ordinary Portland cement (OPC), resulting in a high carbon footprint[3]. To address this, supplementary cementitious materials (SCM) are used for their low embodied carbon and durability benefits. For instance, engineered cementitious composites (ECC) can maintain stable 100-μm cracks using 55% fly ash.

While previous studies have examined cement replacement up to 96%[4], it remains unclear whether FRCCs can sustain effective self-healing in such low-carbon matrices, which often lack the calcium ions necessary for portlandite and subsequent calcite formation.

This study hypothesizes that incorporating cellulose fibers densely coated with nanocalcite particles, supplied in a slurry (referred to as "liquefied pulp"), will act as an internal moisture reservoir[5] and provide vital nucleation sites for calcite precipitation. This mechanism aims to overcome the limited reactivity inherent in developing low-carbon FRCC (LCFRCC) mixes. Furthermore, it should synergize with polyvinyl alcohol (PVA) fibers to promote self-healing through the recovery of watertightness.

To test this hypothesis, this study evaluates the embodied carbon and mechanical performance of developed LCFRCC mixes, examines self-healing behavior through sorptivity, VPV, and Raman spectroscopy using liquefied pulp as a healing agent, and evaluates self-healing performance while accounting for inherent hydration-related changes.

2. Experiment Overview

The experimental program categorized the FRCC mixtures into three series: a conventional ECC mix (C45) with 55% fly ash as a control, and two LCFRCC mixes (C5a and C5b) with 95% cement replacement. All mixes utilized an effective water-to-binder ratio of 0.26 and 2% PVA fibers by volume. With silica fume (SF) fixed at 5% of the binder mass, C5a and C5b varied only by their ground granulated blast-furnace slag (GS) to fly ash (FA) ratios, 2.0 and 0.64, respectively. Each mix was dosed with liquefied pulp (P) at 0% (control), 3%, 6%, or 9%, resulting in 12 combinations for the investigation of autogenous self-healing.

東北大学大学院都市・建築学専攻，ライフサイクル工学分野
Life Cycle Engineering Laboratory,
Dept. of Architecture and Building Science, Tohoku University

Table1 Design mix proportion

Mix Series	B (%wt)				Per B (%wt)				F (%vol)
	C	FA	GS	SF	S	W'*	SP	P	PVA
C45-P0	45	55	0	0	36	25.3	1.0	0	2.0
C45-P3						22.1		3	
C45-P6						18.9		6	
C45-P9						15.8		9	
C5a-P0	5	30	60	5	36	25.7	0.5	0	2.0
C5a-P3						22.5		3	
C5a-P6						19.3		6	
C5a-P9						16.1		9	
C5b-P0	5	55	35	5	36	25.7	0.5	0	2.0
C5b-P3						22.5		3	
C5b-P6						19.3		6	
C5b-P9						16.1		9	

*W' = 26 – 0.70SP – 1.06P

Table 2 Emission factors of constituents[3),6),7)]

Constituent Materials	Emission Factor (kg CO_2 / kg)
OPC	0.84 – 1.1
FA	0.0 – 0.01
GS	0.026 – 0.14
SF	0.014 – 0.028
S	0.0233 – 0.0330
PVA	1.7 – 3.6
SP*	2.25
P*	0.508

*Based on solid content

2.1 Materials and Mix Design

Table 1 details the proportions of the 12 mixtures by percentage of binder mass. The LCFRCC utilized a four-component (quaternary) binder system. The OPC used has a specific gravity (SG) of 3.16 and specific surface area (SSA) of 3,280 cm^2/g and replaced by 95% binder mass with the following SCMs: FA (SiO_2 = 60%; SG = 2.26; SSA = 4,460 cm_2/g), GS (SG = 2.26; SSA = 3,990 cm_2/g), and undensified SF (SiO_2 > 94%; SG = 2.20; SSA = 15,000 – 35,000 cm^2/g). Dry silica sand (SiO_2 = 93.5%, SG = 2.59; 150 µm size) was used at 36% of the binder mass. The fiber reinforcement consisted of oil-treated PVA fibers, manufactured by Kuraray (12 mm length; 40 µm diameter; nominal tensile strength of 1,560 MPa; Young's modulus of 41 GPa; and density of 1.30 g/cm^3). A polycarboxylate-based superplasticizer (SP) with density ranging from 1.05 to 1.13 g/cm^3 was added to achieve a flow value of at least 180 mm, sufficient for uniform fiber dispersion.

The liquefied pulp (MinerPa, manufactured by Nippon Paper Industries) served as the healing agent (wet density = 0.94 – 0.98 g/cm^3). This product consists of softwood-based cellulose (Ø 20 µm) densely coated with nanocalcite particles (0.20 µm) by up to 90% by mass using a patented ultrafine bubble generation method.

Mixing was performed in a 5-L "omni-mixer." First, water was pre-blended with the SP and liquefied pulp to create a uniform suspension. Binders and sand were dry-mixed for one minute at moderate speed (240 rpm), followed by the addition of the pre-blended water and three minutes of mixing at full speed (480 rpm). To prevent agglomeration, PVA fibers were added in three portions, with each portion mixed for one minute at full speed. For the 6% and 9% P dosages, mixing was extended by 1.5 and 3 minutes, respectively, to ensure fiber dispersion and achieve a "creamy" consistency. Flowability, air content, and temperature were checked for quality control. Flow values were obtained conforming to JIS R 5201.

Freshly mixed FRCC was cast into non-absorbent cylindrical molds (Ø 50 × 100 mm) and consolidated using five seconds of vibration. The specimens underwent a steam-curing cycle with a three-hour peak at 65°C inside a sealed container. The specimens were placed above the water at a level low enough to achieve saturated vapor condition. After one day, the specimens were demolded and moist-cured (20°C, >95% RH) for an additional 13 days.

2.2 Viability Check of LCFRCC Mix

This section briefly confirms the viability of the proposed LCFRCC mixes in terms of embodied carbon reduction and basic mechanical performance, prior to detailed self-healing evaluation. The embodied carbon of C5a and C5b mixes were compared to C45 mix using the emission factors listed in Table 2. Additionally, the effect of P dosage was investigated. Following fresh state characterization, the 14-day compressive strength was tested according to JIS A 1108:2018. A hydraulic universal testing machine (YU-1000SIV, manufactured by Tokyo Koki) was employed at a constant loading rate of 0.6 $N/mm^2/s$.

2.3 Preparation of Test Specimens

After 14 days of curing, the cylindrical samples were oven-dried at 60°C for four days. During crack induction for the damaged group, the undamaged group was stored in a desiccator with soda lime pellets to prevent premature carbonation and serve as a baseline for inherent changes during subsequent water immersion. For the damaged group, cracks were introduced via splitting tensile loading (Figure 1) under deformation control within a 5 × 12 mm gauge zone. Loading was terminated at a 0.40-mm displacement, resulting in residual displacements around 0.30 mm. The load-deformation response confirmed the formation of multiple cracks.

Subsequently, both groups were immersed in Grade A3 deionized water (JIS K 0557) at 20°C for 28 days. Dissolved CO_2 concentrations were estimated from hourly ambient CO_2 and temperature data using Henry's Law, with trends smoothed via STL decomposition in R. The pH was monitored weekly, and water levels were maintained.

2.4 Procedure for Self-Healing Assessment

Autogenous self-healing was evaluated through watertightness recovery using both sorptivity and VPV. Both indicators were measured before (D0) and after (D28) immersion on three damaged and three undamaged specimens. Additionally, Micro-Raman spectroscopy was performed on selected crack surfaces within the P0 and P3 mixes to qualitatively identify healing products and provide microstructural evidence of the healing mechanism.

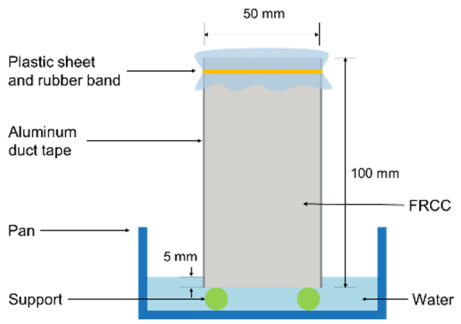

Fig. 2 Set up for sorptivity test

Fig. 3 Vacuum saturation using desiccator

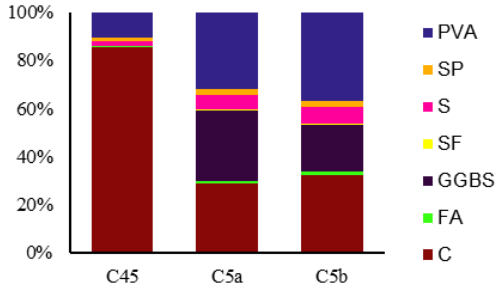

Fig. 4 Contribution of constituents to total embodied carbon

2.4.1 Sorptivity

Sorptivity was measured as the rate of water uptake via unidirectional capillary suction conforming to ABNT NBR 9779, using the setup illustrated in Figure 2. Oven-dried specimens were placed in contact with 5 mm of water at 20°C for tested at D0 and retesting at D28 . During the D0 test, specimens remained unsealed, and mass gain was recorded for 121 minute. For the D28 test, the specimens were sealed with aluminum tape and the top surfaces were covered with plastic sheet. Water absorption (I, mm), was calculated as the mass gain per unit area, with the sorptivity (S, mm/√min) determined from the slope of the linear regression of I against the square root of time (√t, √min).

2.4.2 Volume of Permeable Voids

The VPV was measured according to ASTM C642, modified by replacing the boiling procedure with vacuum saturation at -0.98-MPa (Figure 3) for a minimum of 6 h to ensure filling the finer pores.

To ensure full saturation prior to vacuum treatment, specimens were pre-immersed in water for three days. The oven-dry mass (m_d), saturated surface-dry mass (m_s) after vacuum treatment, and apparent mass in water (m_a) were recorded, assuming a water density (ρ_w) of 1.0 g/ cm^3. The dry bulk density, ρ_b (g/cm^3) was calculated using Equation (1).

Similarly, the VPV, V (%), defined as the percentage of interconnected pore space and/or cracks within the total volume, was calculated using Equation (2). Densification refers to the increase in bulk dry density between D0 and D28.

$$\rho_b = \frac{m_d}{m_s - m_a} \cdot \rho_w \quad (1)$$

$$V = \frac{m_s - m_d}{m_s - m_a} \cdot 100\% \quad (2)$$

2.4.3 Raman Spectroscopy

Micro-Raman spectroscopy (JASCO NRS-5100) was performed on sectioned samples (Ø 50 × 50 mm). To minimize fluorescence, a near-infrared laser (784.67 nm) was focused on the healing product using a 100× objective (1.064 µm spot size) at 4.2 mW. Spectra were acquired over 300 - 1200 cm^{-1} (20 s per scan, 10 accumulations) to identify carbonate and hydrate phases based on established literature.

2.5 Performance Metrics for Evaluation

Standard recovery efficiency fails to isolate inherent changes caused by continued hydration[5]. By testing undamaged specimens, the influence of hydration was accounted for, facilitating for a more accurate assessment of the self-healing process. Using the watertightness parameter, f (either sorptivity or VPV), performance was evaluated via the healing rate (η, Equation (3)) relative to hydration-related change (H, Equation (4)). A positive H value implies pore refinement through densification, while a negative value implies pore coarsening via dissolution.

$$\eta = \left(\frac{f_{c28}}{f_{c0}} - 1\right) \cdot 100\% \quad (3)$$

$$H = \left(\frac{f_{u28}}{f_{u0}} - 1\right) \cdot 100\% \quad (4)$$

3. Development and Characterization of LCFRCC

The C45 control mix has an embodied carbon value of 649 kg-CO_2e/m^3. In contrast, the LCFRCCs achieved carbon reductions of 67% to 71%, with the greater reduction observed in the fly ash-rich mix (C5b). The addition of liquefied pulp has a negligible impact, contributing less than 1 kg-CO_2e/m^3 for every 3% increase in dosage. Figure 4 illustrates the carbon contributions of the primary constituents, excluding liquefied pulp.

Liquefied pulp generally decreased flowability, except for C5a-P3; however, all mixes converged at a flow value of approximately 180 mm at the P9 dosage. The mix series were categorized by observed air content: C45 (~4%), C5b (~3%), and C5a (~2%), with C5a-P3 exhibiting the lowest content at 1.6%. Notably, the C5a series showed higher flow values than both the C45 and C5b mixes across all dosages, with C5a-P3 reaching 264 mm in the 15-shot flow table test.

All mixtures exceeded a 14-day compressive strength of 20.7 MPa, typical for general construction applications. While the LCFRCCs exhibited lower strength than the C45-P0 control (46.2 MPa), the strength of the C5a series improved at dosages exceeding 3%, eventually reaching 35.1 MPa for C5a-P9.

4. Calcite-Coated Cellulose as Healing Agent

Damage induction resulted in residual deformations between 236 and 311 µm. While multi-cracking occurred in all samples, the C45-P6 and C45-

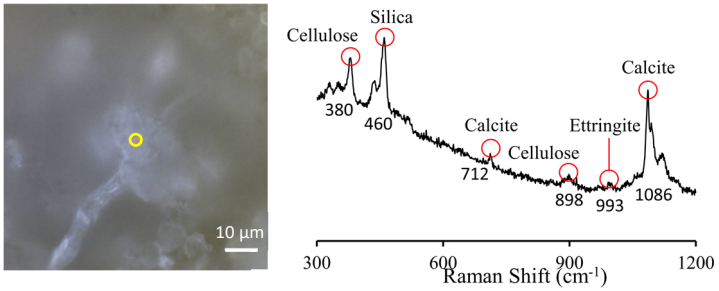

Fig. 5 Optical image and Raman spectra of C45-P3

P9 mixes exhibited maximum crack widths exceeding 300 µm outside the gauge area. In contrast, LCFRCCs demonstrated superior crack width control. During immersion period, the pH remained above 8.0, creating conditions conducive to calcite precipitation. Furthermore, dissolved CO_2 levels fluctuated near 0.80 mg/L and well below 1.0 mg/L.

C45-P0 and C5a-P0 exhibited sorptivity reductions of 68% and 56%, respectively, both converging to 0.12 mm/√min. During immersion, C5a and C5b showed susceptibility to leaching (dissolution of portlandite). The incorporation of liquefied pulp proved ineffective for the C5a series due to the formation of new capillary pathways; however, C5b-P3 effectively mitigated leaching, achieving a 47% reduction in sorptivity.

The VPV at D28 was measured for damaged specimens, with the lowest values in each base mix series observed in C45-P0 (8.6%), C5a-P0 (8.9%), and C5b-P3 (10.4%). While no specimens reached the undamaged VPV levels at D28, the smallest gaps were observed in C45-P3 (0.7%) and C5b-P3 (0.9%). These mixes also exhibited the highest gains in dry bulk density.

Comparing P0 and P3 dosages, Micro-Raman spectroscopy revealed that autogenous self-healing was primarily driven by crystalline calcite precipitation, identified by prominent peaks at 712 and 1085 cm^{-1}, except in C5a-P0 where matrix densification mainly contributed to the crack closure via void refinement despite leaching. Figure 5 shows a dense encrustation of calcite surrounding the cellulose fiber in optical micrograph of C45-P3, revealing the nucleation effect.

5. Evaluation of Self-Healing Performance

In the case of η- H plot for sorptivity (Figure 6), the clustering showed C45 series benefited from self-healing and the capillary pore refinement, outperforming the LCFRCCs. In the C5a series, the pore coarsening was evident but was exacerbated by the liquefied pulp. Conversely, in the C5b series, the P dosages between 3 and 6% promoted pore refinement.

In the case of η- H plot for VPV (Figure 7), the self-healing process proceeded at 85% of the inherent matrix densification kinetics ($R^2 \approx 0.97$). Four mixes achieved or exceeded this 85% mark: C45-P0 (89%), C45-P3 (104%), C5a-P3 (93%), and C5b-P3 (85%), revealing that C45-P3 and C5a-3 benefited more from pore connectivity reduction, which is more important for long-term durability. Comparison of these results provides evidence that liquefied pulp modified the pore structure differently depending on the GGBS/FA ratio. Specifically, the C5b-P6 mix favored refinement of capillary pores over reduction of pore connectivity. Among the LCFRCCs, the C5b series showed the optimum refinement of both pore structures.

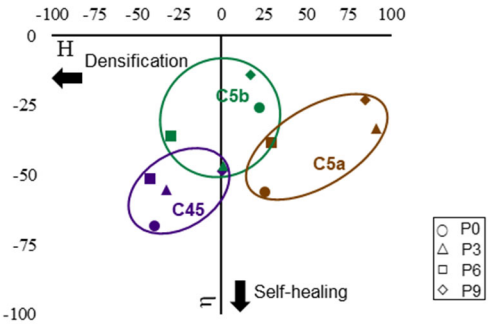

Fig. 6 Self-healing and densification on sorptivity

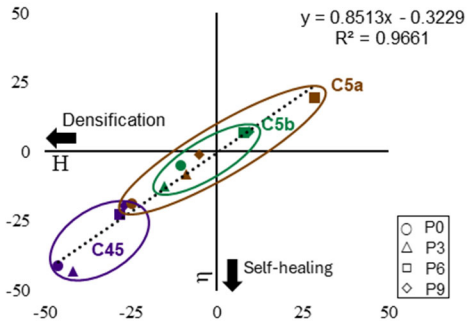

Fig. 7 Self-healing and densification on VPV:

6. Conclusion

This study developed an LCFRCC mix with a 71% lower carbon footprint than conventional ECC by replacing 95% of cement while maintaining practical strength. Although the low-reactivity matrix was prone to leaching, 3% calcite-coated cellulose slurry effectively recovered watertightness in fly-ash-rich binders. These results support the hypothesis that calcite-coated cellulose fibers can compensate for limited reactivity in LCFRCCs by enhancing autogenous self-healing. Analysis of undamaged specimens for baselining further confirmed that this liquefied pulp achieves healing rates exceeding inherent matrix densification, whether viewed through the lens of capillary porosity (sorptivity) or pore connectivity (VPV). This reveals the need to optimize GGBS/FA and PVA-pulp ratios to maximize the additive's efficacy across both pore structures.

References

1) Zhang, W. et al.: Self-healing cement concrete composites for resilient infrastructures: A review, *Composites Part B: Engineering*, **189**, 107892, 2020
2) Nishiwaki, T. et al.: Experimental study on self-healing capability of FRCC using different types of synthetic fibers, *Journal of Advanced Concrete Technology*, **10**(6), 195–206, 2012
3) Shoji, D. et al.: The greening of engineered cementitious composites (ECC): A review, *Construction and Building Materials*, **327**, 126701, 2022
4) Yao, C. et al.: Review on autogenous self-healing technologies and multi-dimension mechanisms for cement concrete, *Archives of Civil and Mechanical Engineering*, **24**, 15, 2024
5) 鈴木南都ら：CO_2排出量削減を実現するセメントコンクリートの開発と評価，コンクリート工学年次論文集, **45**(1), 1054–1059, 2023
6) Schiefer, C. and Plank, J.: On the CO2 footprint of polycarboxylate superplasticizers (PCEs) and its impact on the eco balance of concrete, *Construction and Building Materials*, **409**, 133944, 2023
7) Sun, M. et al.: Uncovering energy use, carbon emissions and environmental burdens of pulp and paper industry: A systematic review and meta-analysis, *Renewable and Sustainable Energy Reviews*, 92, 823–833, 2018